ELSEVIER

Nuclear Instruments and Methods in Physics Research A 362 (1995) 454–465

NUCLEAR INSTRUMENTS & METHODS IN PHYSICS RESEARCH
Section A

Measurements of response function of organic liquid scintillator for neutron energy range up to 135 MeV

Noriaki Nakao [a,1], Takashi Nakamura [a,*], Mamoru Baba [b], Yoshitomo Uwamino [c], Noriyoshi Nakanishi [c], Hiroshi Nakashima [d], Shun-ichi Tanaka [d]

[a] *Cyclotron and Radioisotope Center, Tohoku University, Aoba, Aramaki, Aoba-ku, Sendai, 980 Japan*
[b] *Department of Nuclear Engineering, Tohoku University, Aoba, Aramaki, Aoba-ku, Sendai, 980 Japan*
[c] *Institute of Physical and Chemical Research, Hirosawa, Wakou-shi, Saitama, 351-01 Japan*
[d] *Tokai Establishment, Japan Atomic Energy Research Institute, Tokai-mura, Naka-gun, Ibaragi, 319-11 Japan*

Received 23 January 1995

Abstract

Neutron response functions of 12.7 cm diameter by 12.7 cm long BC501A organic liquid scintillator have been measured for energy range up to 135 MeV continuously with the TOF method. The measured response functions were compared with Monte Carlo calculations using some codes which are widely used. The comparison showed good agreement below 20 MeV, but some discrepancy above 20 MeV, owing to the inaccurate cross sections of carbon reactions and light yields of produced charged particles. Finally, the new response matrix which covered from 0 to 120 MeV based on the measured data was constructed by the help of calculation data.

1. Introduction

Accelerators have recently been used not only for nuclear physics and material science but also for industrial and medical uses. The number of more intense and higher energy accelerators is therefore increasing, which increases the importance of studies on shielding design and experiments of high energy neutron shielding. Organic liquid scintillators such as NE213 and BC501A are widely used for spectroscopy of high energy neutrons because of high detection efficiency, good n–γ discrimination capability, comparably good resolution and fast decay time of the scintillation.

The scintillation light outputs measured with the scintillator are converted into neutron energy spectra using the time of flight (TOF) method or unfolding method, which requires the response functions of the scintillator. Especially, for unfolding method the response functions have to be given with good accuracy to avoid the nonphysical oscillation or distortion of the unfolded spectra.

Lots of experimental studies on neutron detection efficiencies and charged particle light yields in the hydrocarbon scintillators have been done for a long time, and the reproductions for the distributions of differential light outputs from the scintillators have been calculated using the Monte Carlo method. A couple of Monte Carlo codes, such as O5S [1] and SCINFUL [2] which were developed in ORNL, and CECIL revised by Cecil et al. [3] from the Stanton code [4], and RESU by Uwamino et al. [5], are widely used to calculate the neutron response functions. These codes indicated that all of them pretty well reproduce the light distributions, that is response functions, for less than about 20 MeV neutrons, however, for higher neutron energy have large discrepancies from the measured distributions owing to the complexity of carbon reactions and inaccurate light yields of charged particles in the scintillator. It is then necessary to get experimental response functions in good accuracy for spectrum unfolding.

Several experimental results of neutron response functions above 20 MeV for organic liquid scintillators have been reported [5–8], but in this study we have measured the response functions of BC501A to neutrons of 5 to 135 MeV energies in good accuracy by using the TOF method in three cyclotron facilities. The response functions were given in a matrix form for general use.

2. Measurement

2.1. Detector

The detector calibrated in this work is cylindrical organic liquid scintillator of 12.7 cm diam by 12.7 cm long

* Corresponding author.
[1] Present address: Institute for Nuclear Study, University of Tokyo, Midori-cho, Taneshi, Tokyo 188, Japan.

0168-9002/95/$09.50
SSDI 0168-9002(95)00193-X

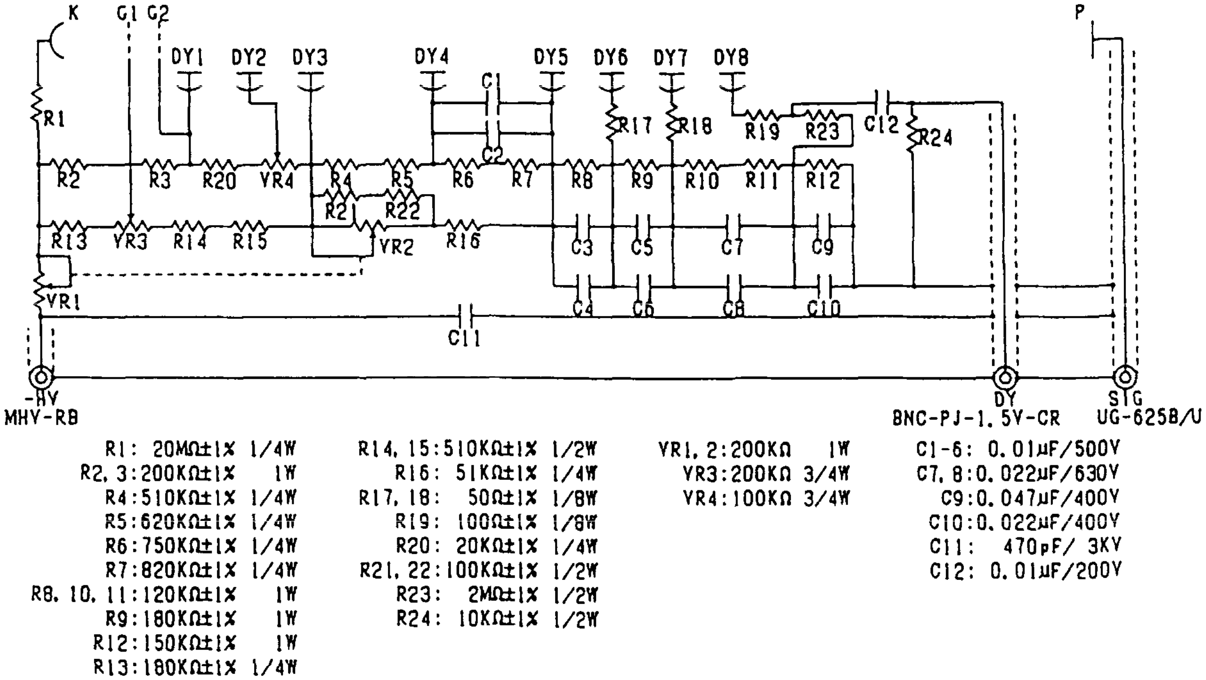

Fig. 1. Circuit of the R4144 photomultiplier base connected to BC501A scintillator.

BC501A (BICRON Co. Ltd.). The density and the composition of the scintillator are 0.874 g/cm^3 and $CH_{1.212}$, respectively.

This scintillator is coupled to a R4144 photomultiplier connected to E1458 base (Hamamatsu Photonics. Co. Ltd.) which is designed to expand the dynamic range of output pulses for high energy neutron measurements, as shown in Fig. 1.

The detector size which stops the recoil proton up to about 120 MeV was selected in order to be able to detect as higher energy neutrons as possible with keeping a good n–γ pulse-shape discrimination capability.

2.2. Neutron sources

The neutron response functions of the scintillator were measured in three cyclotron facilities, Cyclotron and Radioisotope Center (CYRIC) in Tohoku University, Takasaki Ion Accelerator for Advanced Radiation Application Facility (TIARA) in Japan Atomic Energy Research Institute, and Institute of Physical and Chemical Research (RIKEN), under the six projectile–target combinations, which are listed in Table 1.

For the top five experiments, white spectral neutrons were generated from these targets which were thick enough to stop accelerated particles, and the last experiment used quasi-monoenergetic neutrons produced from thin Li target. The light output distributions of the scintillator to neutrons in wide energy range were measured by grouping white spectral neutrons into monoenergetic interval with the TOF method. The neutrons generated at 0° were used in all measurements. These neutron spectra are shown in Figs. 2 to 4. The detection efficiencies for the TOF measurements were obtained from the response matrix of the final results in this work.

Table 1
Projectile–target combinations which generated source neutrons

Facility	Projectile	Target (thickness [mm])	Repetition rate	Flight path [m]
CYRIC	35 MeV-p^+	^{9}Be (10)	425.2 ns	11.56
CYRIC	50 MeV-$^3He^{2+}$	^{9}Be (10)	404.6 ns	11.47
CYRIC	65 MeV-$^3He^{2+}$	^{9}Be (10)	400.8 ns	10.57
TIARA	67 MeV-p^+	Cu (7.6)	317.1 ns	13.47
RIKEN	135 MeV-p^+	^{9}Be (70) + C (20)	40 μs	13.17
RIKEN	135 MeV-p^+	^{7}Li (5)	40 μs	13.17

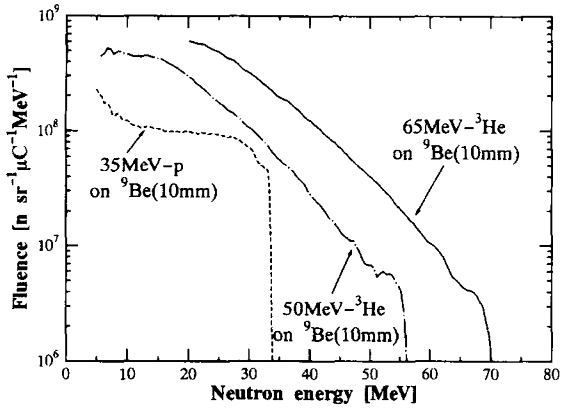

Fig. 2. Source neutron spectra at 0° used for response function measurements in CYRIC.

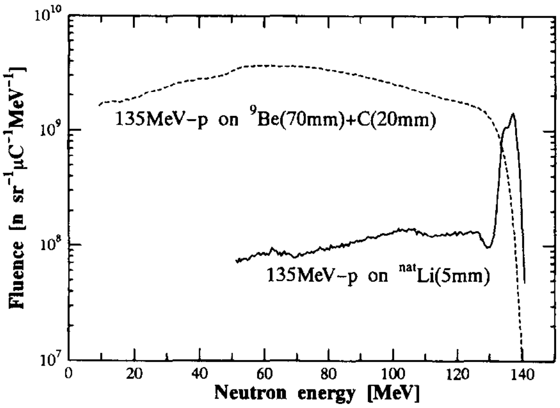

Fig. 4. Source neutron spectra at 0° used for response function measurements in RIKEN.

In order to measure the response functions down to a few MeV neutron energy, the repetition rate of the projectile beam in these measurements was reduced to be longer than a few hundreds ns by chopper. These repeated experiments were used to check the reproducibility and the accuracy of the obtained results.

2.3. Experimental setup

These measurements were done under the geometry that the detector was located on the neutron beam line downstream from the target. The flight paths in each measurement are also shown in Table 1.

Fig. 5 shows the experimental arrangement at the TOF facility of CYRIC. Protons accelerated to 35 MeV and $^3He^{2+}$ ions accelerated to 50 and 65 MeV were injected into a 10 mm thick ^{9}Be target. Although the accelerated ions were fully stopped in the target, the charged particles generated in the target, for example, protons from ^{9}Be(^{3}He, p) reaction, passed through the target and the 10 mm thick aluminium Faraday cup placed behind the target. Only in the 65 MeV $^3He^{2+}$ beam run, another 5 mm thick Al plate to absorb these charged particles was attached just behind the Faraday cup. The neutrons generated at 0° were transported into the TOF room through first and second collimators shown in Fig. 5, and were detected by the scintillator.

Fig. 6 shows the experimental arrangement at the AVF cyclotron facility of TIARA. In TIARA, 67 MeV proton beam was injected into the 7.6 mm thick copper target to produce white spectral neutrons. The charged particles produced in the target were bent down to the beam dump by the clearing magnet. The neutrons emitted in the forward direction were extracted into the experimental room through the cylindrical iron collimator of 10.9 cm diameter and 220 cm length.

Fig. 7 shows the experimental arrangement at the ring cyclotron of RIKEN. In RIKEN, H_2^+ ion beam of 135 MeV/nucleon energy was injected into the Be (70 mm thick) + C (20 mm thick) target to produce white spectral neutrons and the 5 mm thick natural Li target to produce

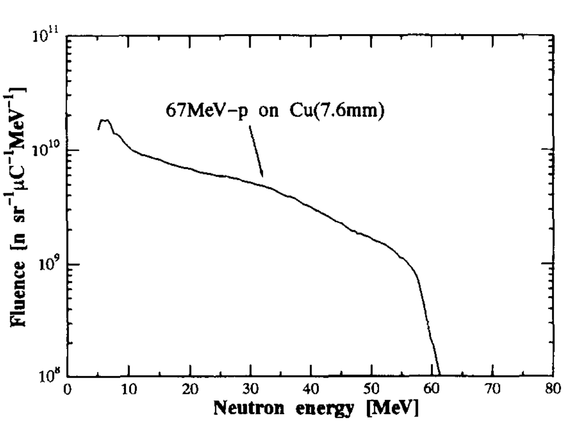

Fig. 3. Source neutron spectra at 0° used for response function measurements in TIARA.

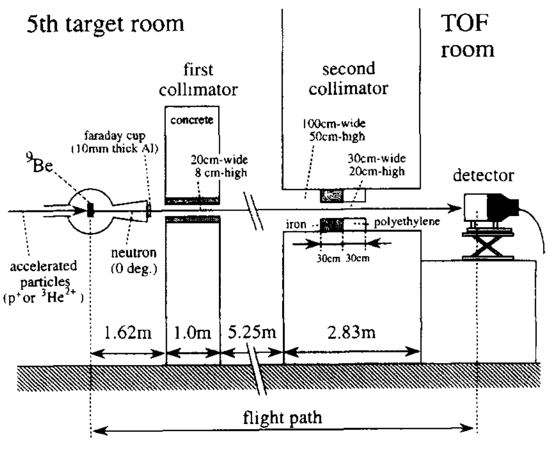

Fig. 5. Experimental setup in CYRIC.

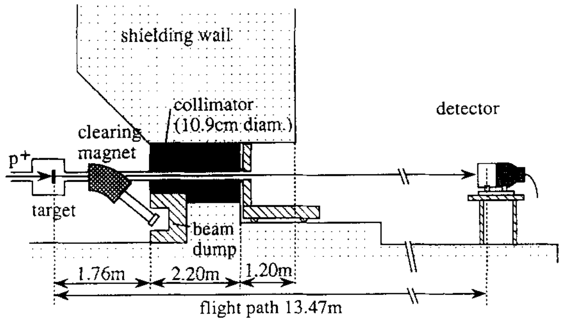

Fig. 6. Experimental setup in TIARA.

quasi-monoenergetic neutrons. The charged particles which penetrated the thin target or produced in the target were transported to the beam dump by the dipole bending magnet. The neutrons emitted in the forward direction were measured with the detector through the collimator of 20 cm × 20 cm aperture and 120 cm length.

2.4. Measuring circuit

Fig. 8 illustrates the block diagram of the measuring circuits in the CYRIC experiment as an example. At TIARA and RIKEN, the similar circuits were used for neutron TOF measurements. The output pulses from the dynode were amplified through a delay-line amplifier and divided into two; one was fed to a delay amplifier to supply light output (energy proportional) pulses and the other fed to a rise time-to-height converter to supply rise time pulses which were used for n–γ pulse shape discrimination. The fast output pulses from the anode were used as the start signal to get the TOF outputs by combining the chopped trigger signal from the cyclotron as the stop signal. These three pulses were recorded in the list mode of the CAMAC system.

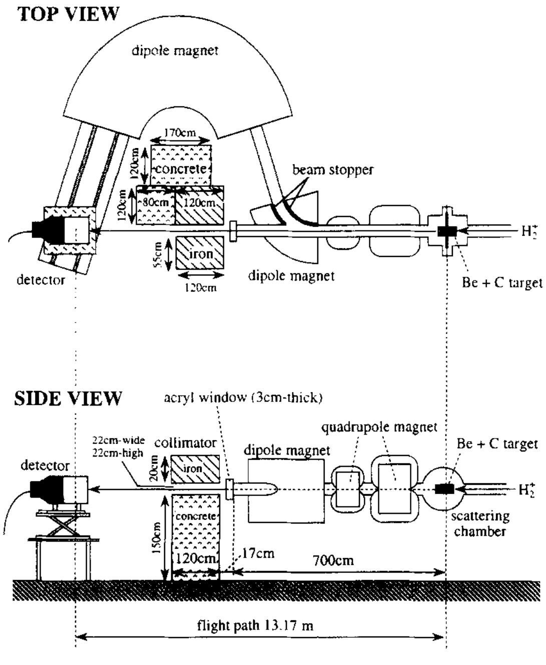

Fig. 7. Experimental setup in RIKEN.

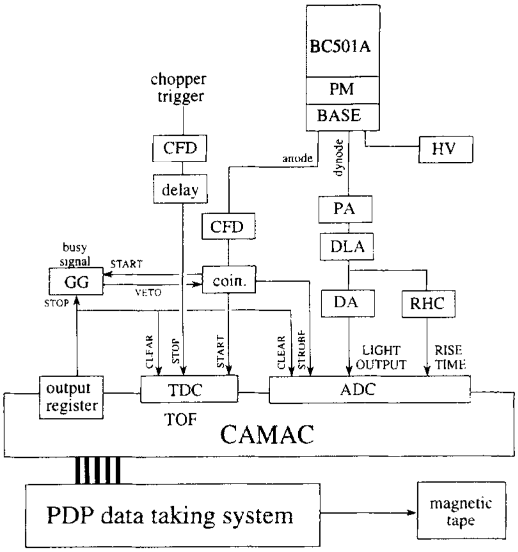

Fig. 8. Block diagram of measuring circuits. PA: preamplifier, DLA: delay line amplifier, DA: delay amplifier, RHC: rise time-to-height converter, CFD: constant fraction discriminator, GG: gate generator, TDC: time-to-digital converter, ADC: analog-to-digital converter.

3. Analysis

3.1. Time resolution

The TOF spectrum was converted to the energy spectrum. Time resolutions of the TOF measurements were determined from the FWHM of γ-ray peak (ΔT_γ) flashed from the target and are shown as 1.22 to 1.78 ns in Table 2.

Table 2
Time resolution estimated from FWHM of γ-ray peak flashed from the target in the TOF measurements

Measurement			Time resolution ΔT_γ [ns]
CYRIC	35 MeV	p	1.22
CYRIC	50 MeV	^{3}He	1.25
CYRIC	65 MeV	^{3}He	1.22
TIARA	67 MeV	p	1.78
RIKEN	135 MeV	p	1.55

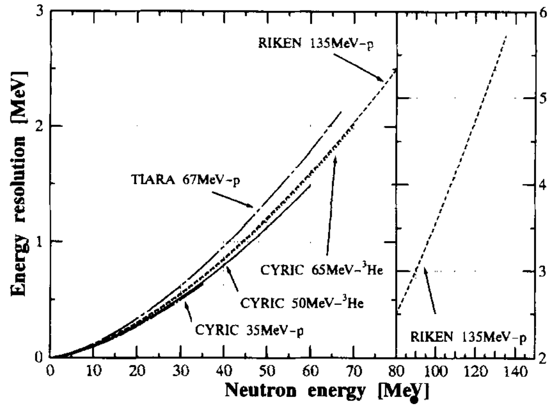

Fig. 9. Neutron energy resolution estimated from the time resolution.

Neutron energy resolutions ΔE, shown in Fig. 9, were estimated by using the following formula as a function of neutron energy E,

$$\Delta E(E)$$

$$= \left(E + M_0c^2\right)\frac{\beta(E)^2}{1-\beta(E)^2}$$

$$\times\sqrt{\left(\frac{\Delta L}{L}\right)^2 + \left(\frac{\Delta T(E)}{T(E)}\right)^2},$$

$$\simeq \left(E + M_0c^2\right)\frac{\beta(E)^2}{1-\beta(E)^2}$$

$$\times\sqrt{\left(\frac{\Delta T_\gamma}{T(E)}\right)^2 + \left(\frac{\Delta T_d(E)}{T(E)}\right)^2}, \quad (1)$$

where M_0 is the neutron rest mass, c the light velocity, $\beta(E)$ the ratio of neutron velocity to light velocity, L the flight path and $T(E)$ the neutron flight time. $\Delta T_d(E)$ is the correction of time resolution difference between neutrons and γ-rays coming from the detector thickness D, which is given by,

$$\Delta T_d = \tfrac{1}{2}D/(c - v(E)), \quad (2)$$

where $v(E)$ is the neutron velocity of energy E. The energy resolution increases with neutron energy to be 5.6 MeV for 132.5 MeV neutrons.

Fig. 10 shows the two-dimensional distribution of light output and rise time for 29–30 MeV neutrons, as an example. The components of charged particles, that is electrons, protons, deuterons and alpha particles, produced

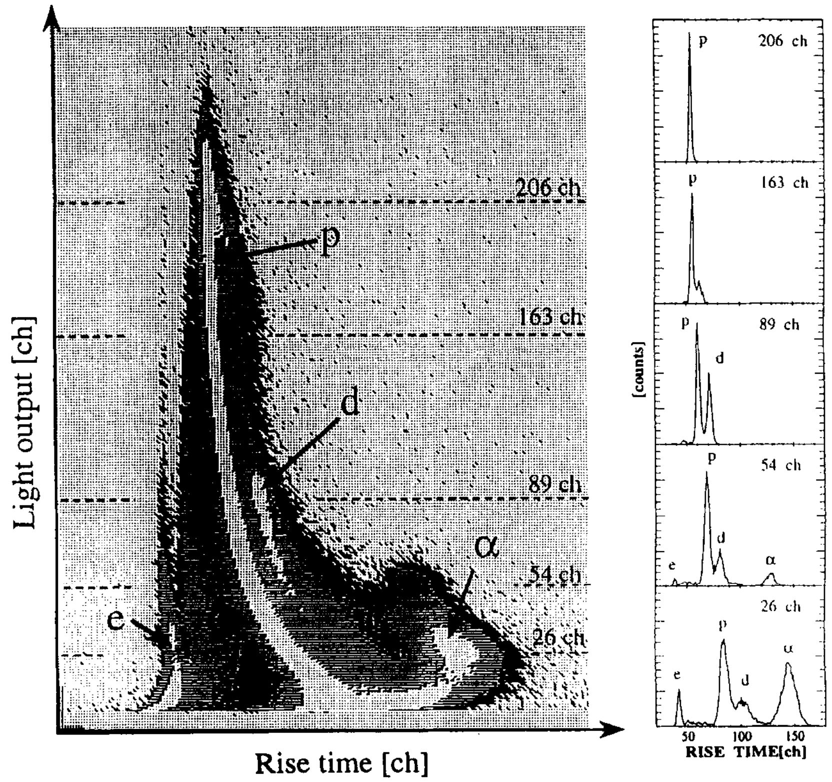

Fig. 10. Two-dimensional view of rise time versus light output in response function measurement gated for 29–30 MeV neutron. The right hand of the figure is the cross-sectional view of rise time distribution at several light output channels.

in the scintillator can be roughly distinguished in the order of rise time. In the right-hand side of Fig. 10, the cross-sectional view of rise time distribution at several light output channels (indicated in Fig. 10) are shown for clear identification of charged particles.

After eliminating electron pulses generated from γ-rays in the two-dimensional light output versus rise time distributions, we selected neutron event data by summing up all other charged particle pulses, and sampled into neutron energy interval which was determined from the neutron TOF measurement. The energy interval widths were fixed to be 1, 2, 4, 5 MeV for neutron energy range from 0 to 44, 44 to 70, 70 to 90, 90 to 130 MeV, respectively, so as to be wider than that of energy resolution shown in Fig. 9. We finally obtained the neutron response functions of the scintillator in the neutron energy range up to 120 MeV.

3.2. Energy calibration

The energy calibration was made in all measurements to convert light outputs into MeV electron equivalent (MeVee) by using the Compton edges of the respective 1.25 and 4.43 MeV γ-rays from ^{60}Co and ^{241}Am–Be, and a pulser was used to define the pulse height channel for the zero-point of light output.

Since the calibration using only γ-ray sources introduced a large error of the calibration for high energy neutron pulses, the recoil proton edges of the response functions obtained above were used for the calibration of proton energy up to 40 MeV. In this process, the proton light yield data by Shin et al. [9] were used, because below 40 MeV proton energy, proton light output curve expressed by Birks' formula [10] well represents the experimental data [5,6].

4. Monte Carlo calculation

In order to compare with the experimental results, calculations of response functions were carried out with three Monte Carlo codes which are widely used. One is the SCINFUL code [2] developed by Dickens. The upper limit of neutron energy which can be calculated in this code is 80 MeV. Second is the RESU code [5] developed by Uwamino et al., which can calculate the response functions for neutron energy range up to 100 MeV. Those upper energy limits depend on the available and reliable limits of the cross section and light yield data. The third code, CECIL is of Cecil et al. [3], which was modified from Stanton code [4]. This code which can calculate the response function up to several GeV neutrons is especially used for calculation of high energy neutron detection efficiency in TOF measurements.

The results of these three codes are expressed as different light output unit. Since MeV electron equivalent (MeVee) is widely used as the unit of scintillator light output, Na unit and Co unit which are used in SCINFUL and RESU codes were converted to 1.25 [6] and 1.27 MeVee [9], respectively.

As the absolute values of light outputs, that is response functions, could not be obtained with the measurements, the measured data were normalized to the corresponding calculated values around the upper plateau edge of the response function, where the neutron reaction in the detector is dominantly the H(n, n) reaction. This normalization can be justified, since the calculated response functions in this high energy end are considered to have good accuracy due to well evaluated H(n, n) cross section values.

In the neutron energy higher than 100 MeV, however, the calculation of response function becomes complicated from the lack of cross section and light yield data, from the difficulty of modeling for various reactions, and from the increasing leakage of the produced charged particles and so on. We therefore developed a simple Monte Carlo code which can estimate the response functions around upper proton edges by considering only the light output from protons recoiled by H(n, n) reaction. The response function values around the upper recoil proton edge can accurately estimate only from total cross section of hydrogen, total and elastic cross sections of carbon determining the reaction probability because all nonelastic reactions of carbon have negative Q-values and the maximum light yield corresponding to the nonelastic reaction is 4.43 MeV less than that of recoil proton.

The cross section data used in our Monte Carlo calculation are shown in Table 3. The ENDF/B-VI [11] and Guerra's compiled data [12] were used for neutron energy range up to 100 MeV, and the eye guides of the cross section curve in Ref. [13] were used for 100 to 200 MeV. The elastic cross sections of carbon in this energy range were obtained by subtracting nonelastic cross sections from the total ones.

The angular distribution of elastic scattering in our code was expressed by the Legendre expansion using coefficients of 16 order from ENDF/B-VI [11] which was compiled up to 100 and 32 MeV in the center-of-mass

Table 3
Microscopic cross section data used for our Monte Carlo code

Cross section	Energy range [MeV]	Reference
H total	~ 100	ENDF/B-VI [11]
	100 ~ 200	Ref. [13]
^{12}C total	~ 32	ENDF/B-VI [11]
	32 ~ 100	Guerra's data [12]
	100 ~ 200	Ref. [13]
^{12}C elastic	~ 32	ENDF/B-VI [11]
	32 ~ 100	Guerra's data [12]
	100 ~ 200	Ref. [13] [a]

[a] Obtained by subtracting nonelastic cross sections from the total ones.

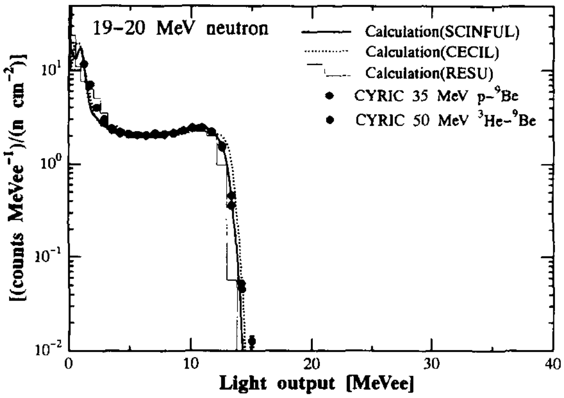

Fig. 11. Measured response functions of BC501A for 19–20 MeV neutron, compared with the calculated results.

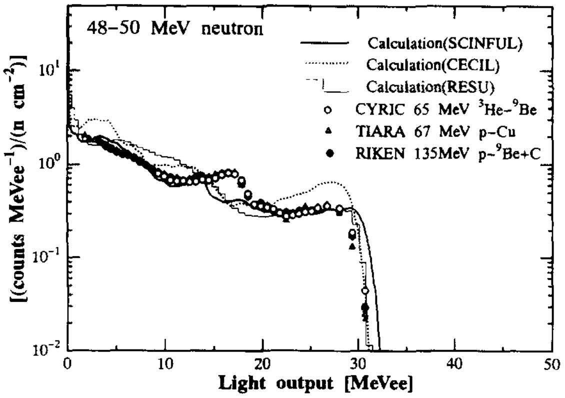

Fig. 13. Measured response functions of BC501A for 48–50 MeV neutron, compared with the calculated results.

system for hydrogen and carbon, respectively. The data for higher energy neutrons were approximated to be the same as those obtained for maximum energy of compiled data. The light yield data of the BC501A scintillator for proton was estimated from the measured light yield described later. The proton range in the BC501A scintillator calculated with the SPAR code [14] was used in the Monte Carlo calculation. In the program, reaction processes were determined by the relativistic kinematics, and the history was terminated when neutrons escaped the detector, neutrons had an energy less than cut-off energy, or the nonelastic scattering occurred.

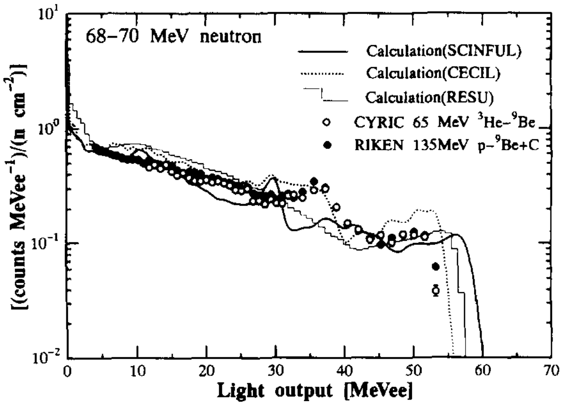

Fig. 14. Measured response functions of BC501A for 68–70 MeV neutron, compared with the calculated results.

5. Results and discussion

5.1. Comparison of measured and calculated response functions

Figs. 11 to 18 show the measured response functions for 19–20, 29–30, 48–50, 68–70, 95–100, 115–120,

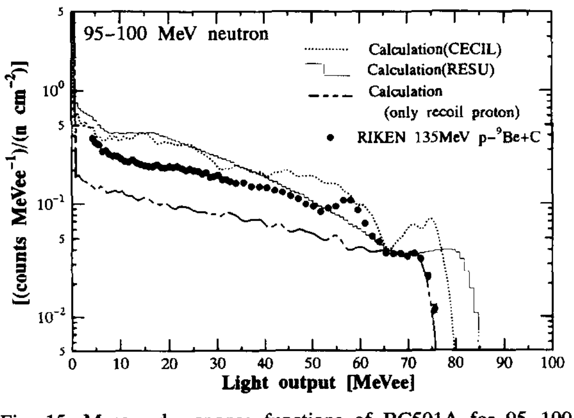

Fig. 15. Measured response functions of BC501A for 95–100 MeV neutron, compared with the calculated results.

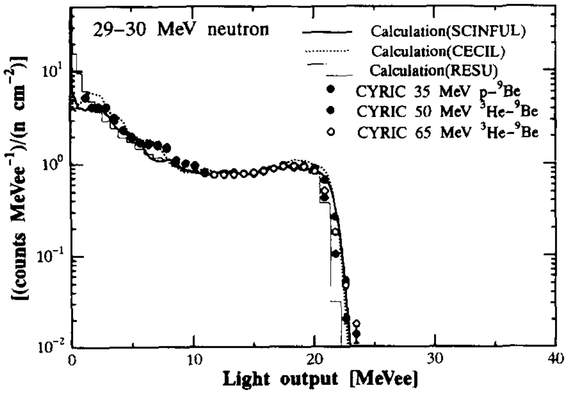

Fig. 12. Measured response functions of BC501A for 29–30 MeV neutron, compared with the calculated results.

120–125 and 132.5 MeV neutrons, respectively, comparing with the calculated response functions. As seen in the figures, the measured results for each neutron energy

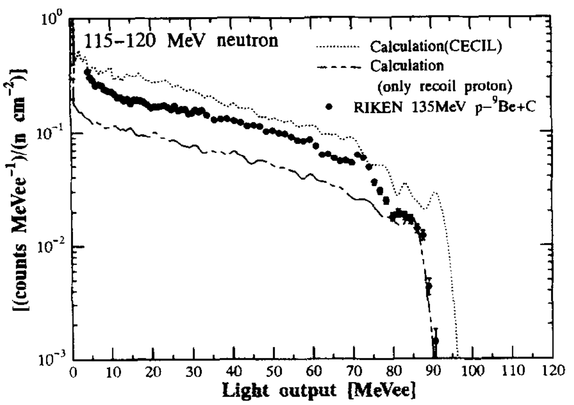

Fig. 16. Measured response functions of BC501A for 115–120 MeV neutron, compared with the calculated results.

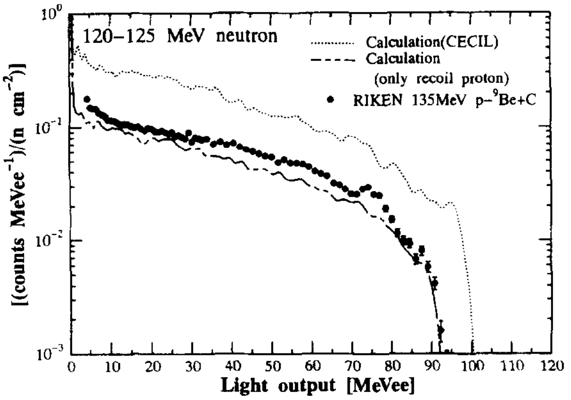

Fig. 17. Measured response functions of BC501A for 120–125 MeV neutron, compared with the calculated results.

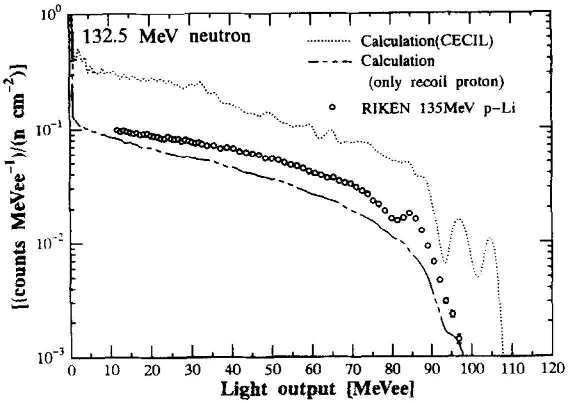

Fig. 18. Measured response functions of BC501A for 132.5 MeV neutron, compared with the calculated results.

interval which were obtained by the five kinds of white spectral neutrons at CYRIC, TIARA and RIKEN listed in Table 1, show extremely good agreement. The absolute values of measured results are obtained by normalization as described in Section 6.

Below 20 MeV, calculated results with three Monte Carlo codes are all in good agreement with the measured results, except a small difference in the upper recoil proton edge.

In the response function for 29–30 MeV neutron shown in Fig. 12, a small discrepancy between measurement and calculation is also found in the middle of the light output distribution. This discrepancy becomes larger for 48–50 and 68–70 MeV neutrons in Figs. 13 and 14, and this middle part tends to have a sharp peak in both calculation and measurement. The results calculated with the CECIL code have a higher efficiency around the upper recoil

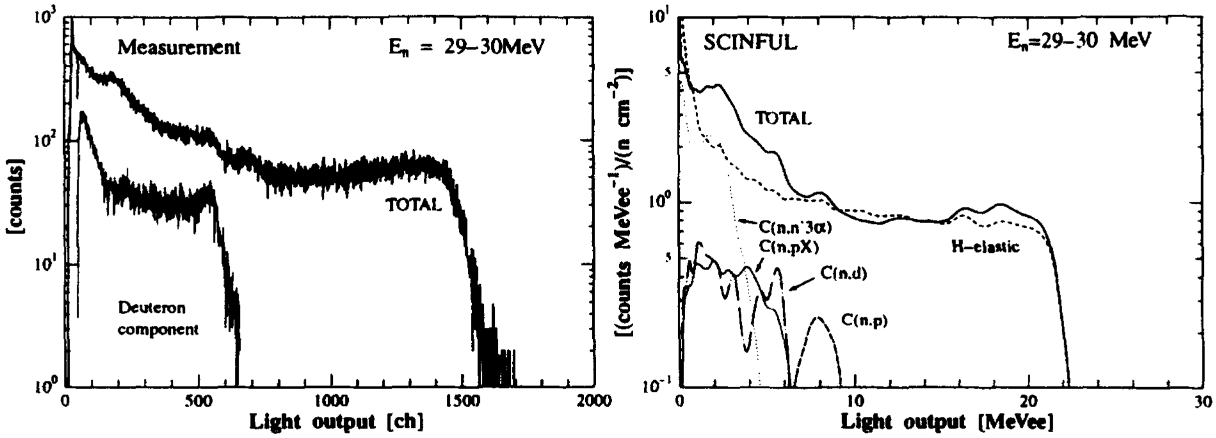

Fig. 19. Summation and components of the light output distributions of charged particles produced from several neutron reactions in the scintillator for 29–30 MeV neutron. Left: total and deuteron component of measured data. Right: calculated with SCINFIL.

proton edge than with the other two codes. Only the SCINFUL calculation gives the middle peak, but the peak position is different from that of the measured results. This middle peak is clearly due to the deuteron component produced in the detector as seen in Fig. 10. The light output distribution due to deuterons was obtained by selecting this deuteron component region from Fig. 10, and is shown in Figs. 19 and 20, comparing with the light output distributions of charged particle components produced from several neutron reactions in the scintillator calculated with the SCINFUL code which can treat the ^{12}C(n, d) reaction. These figures reveal that the middle peaks are due to deuterons, and that the estimation of deuteron light yield is inaccurate in the SCINFUL code. The other two codes cannot treat the ^{12}C(n, d) reaction, therefore the middle peak could not be represented in this calculation.

On the other hand, at the upper recoil proton edge in Figs. 13 to 18, the measured results are considerably lower than the calculated results, which also indicates the inaccurate estimation of proton light yield for higher proton energy.

Fig. 15 shows the response function for 95–100 MeV neutron. The measured light output distribution is much different from two calculated results. The results calculated using the CECIL code has a sharp peak around the upper recoil proton edge while the measured result and the RESU calculation have a flat edge. The proton light output distribution calculated with our developed code showed good agreement around the upper recoil proton edge.

Figs. 16 and 17 show the response functions for 115–120 and 120–125 MeV neutrons, respectively. The proton energy corresponding to the range equal to the scintillator length, 12.7 cm, is about 123 MeV from the calculation with the SPAR code [14]. In this incident neutron energy region, therefore a considerable amount of protons can leak out from the scintillator. The result of the CECIL code is higher than the measured response functions throughout the light output. The results calculated with our developed code agree well with the measured results only around the upper recoil proton edge since the events from carbon reactions in the detector have almost no effect to the upper edge in this neutron energy region.

Fig. 18 shows the response function for 132.5 MeV neutron. The measured data was obtained by using quasi-monoenergetic neutrons generated from 135 MeV/u H_2^+ injected into a thin natural Li target. Beyond 123 MeV energy, the protons recoiled in the forward direction can penetrate the scintillator with depositing a part of their energy, and the slope of the recoil proton edge in the measured response function becomes gentler and the maximum light output is almost the same as that for 125 MeV neutron. On the other hand, the results of the CECIL code has higher recoil proton edge, because this code utilizes the proton range data for PILOT-B scintillator which stops protons of energy range up to about 133 MeV. The result of our code deviated from the measured result even at the upper edge, where charged particles from carbon reactions, especially protons and deuterons from C(n, p) and C(n, d) reactions, has non-negligible contribution to light outputs in this high energy region.

After all, the discrepancy between experiment and calculation comes mainly from that the light yields of produced charged particles are not so accurately estimated in the Monte Carlo code for high energy neutrons. The cross section data and modeling of the carbon reactions, (n, p), (n, d), (n, pn), (n, n′3α) and so on, are also significantly important for high energy neutrons. Furthermore, light attenuation correction in the scintillator should also be considered for a large volume scintillator. Although the SCINFUL code includes the light attenuation correction cited from Kuijper et al. [15], this comparison found that only one parameter for the attenuation calculation is not satisfactory for wide energy range.

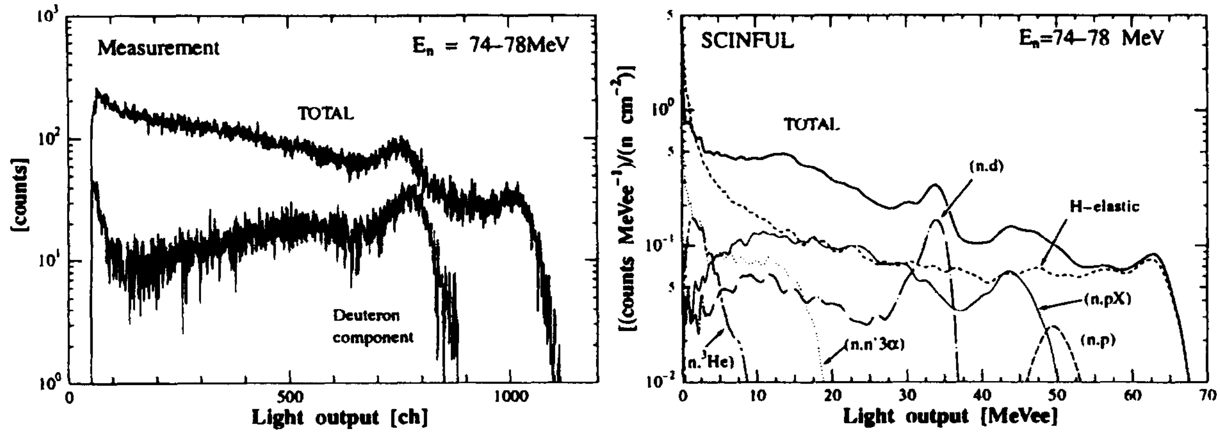

Fig. 20. Summation and components of the light output distributions of charged particles produced from several neutron reactions in the scintillator for 74–78 MeV neutron. Left: total and deuteron component of measured data. Right: calculated with SCINFUL.

5.2. Light yield estimation

From our measurements, the light yield of proton was estimated from the recoil proton edge of response functions. The proton energy recoiled in the forward direction is equal to the neutron energy, since the upper edge of the response function is formed by that proton. The position of the real proton edge was determined to be the position having R-times count of the apparent recoil proton peak. This ratio R was estimated for various neutron energy bins by the help of SCINFUL calculation and exemplified in Table 4. The errors of light outputs were estimated from the width between the apparent recoil proton peak and the real proton edge, and the errors of the proton energy thus determined were also from the width of neutron energy bins of the response functions.

Fig. 21 shows the measured proton light yields together with the errors, comparing with the data compiled in SCINFUL, RESU and CECIL. The light yield data used in SCINFUL and RESU codes are presented by Verbinski et al. [6] and Shin et al. [9], respectively. Both data were obtained up to 100 MeV by fitting their experimental results up to 22 and 15 MeV, respectively, to the Birks'

Table 4
Ratio R of recoil proton peak to real proton edge

Neutron energy interval [MeV]	Recoiled proton energy [MeV]	R
9–10	9.5	0.30
19–20	19.5	0.34
29–30	29.5	0.40
39–40	39.5	0.43
48–50	49.0	0.46
higher than 60	–	0.50

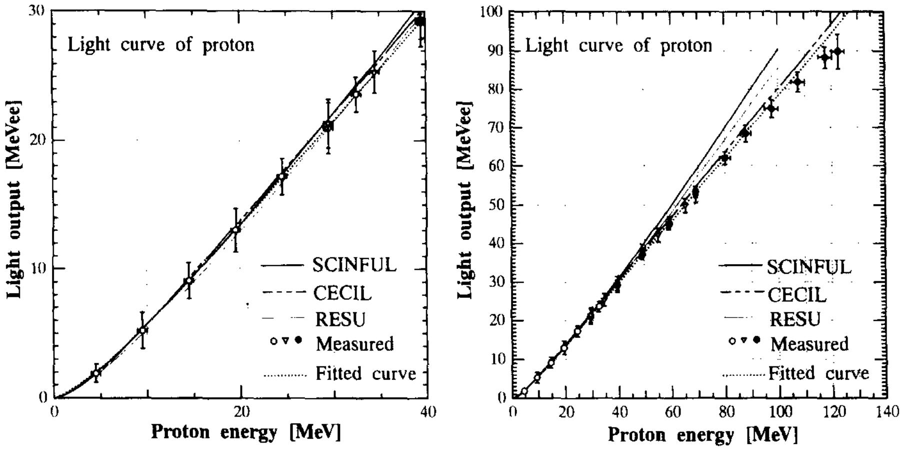

Fig. 21. Light yield of BC501A scintillator to proton. The plots are our measured data and the dotted line is the fitting curve to Eq. (3). The other three lines are the data compiled in the three codes.

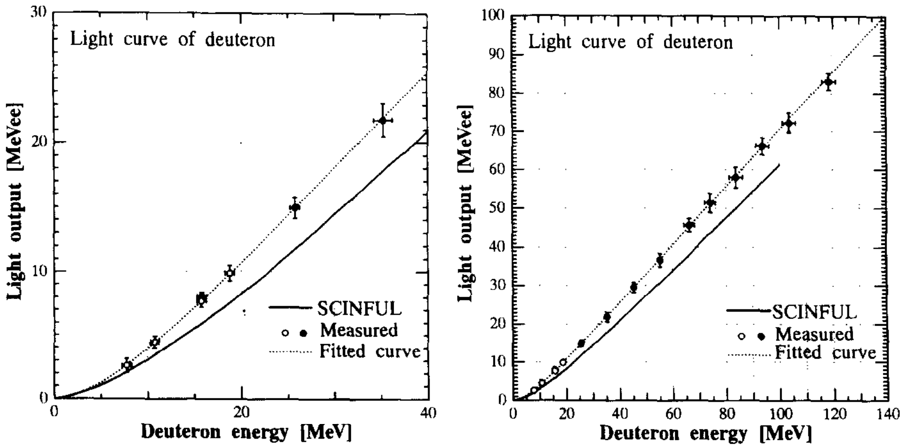

Fig. 22. Light yield of BC501A scintillator to deuteron. The plots are our measured data and the dotted line is the fitting curve to Eq. (3). The other line is the data compiled in SCINFUL.

formula [10]. Our measured results are in good agreement with these data below 40 MeV, but above 40 MeV, our results become lower than those given by SCINFUL and RESU, however, show rather good agreement with the light data of Cecil et al. [3].

By using the following formula which is similar to the formula used in the CECIL code, our measured proton light yields, L [MeVee] were fitted very well over the wide energy range,

$$L = a_1 E_p - a_2\{1.0 - \exp(-a_3 E_p)\}, \tag{3}$$

where E_p [MeV] is the proton energy and the coefficients of a_1, a_2, a_3 are tabulated in Table 5. The light yield curve of proton given by this formula is linearly proportional to proton energy above 10 MeV and agrees well with the measured data below 100 MeV. However, the measured data becomes lower than the fitted curve above 100 MeV owing to light attenuation effect.

The deuteron light yields were also estimated from the upper edge of middle deuteron peak in the response function as shown in Figs. 19 and 20. Since the Q-value of the C(n, d) reaction is -13.73 MeV, the deuteron energies are obtained as

$$E_d = E_n - 13.73 \text{ MeV}. \tag{4}$$

Fig. 22 shows the measured deuteron light yields compared with the data compiled in the SCINFUL code up to 100 MeV. The measured results were also successfully fitted by Eq. (3) and the coefficients are shown in Table 5. Our results are much higher than the data compiled in SCINFUL.

6. Formation of response matrix

Since the absolute values of our measured response functions could not be obtained experimentally as described above, the measured values were normalized to the corresponding calculated values by integrating them from upper recoil proton edge to the light output of a few MeV lower than the edge. The response calculations were done with the SCINFUL code for neutron energies below 78 MeV and with our code for neutron energies from 78 to 120 MeV, from the reason described before. The calculations with SCINFUL were done by changing the original proton light yield data to the measured data, since the light yield in SCINFUL is largely different from the measured

Table 5
Coefficients in Eq. (3) for proton and deuteron

Particle	Coefficient		
	a_1	a_2	a_3
Proton	0.81	2.8	0.20
Deuteron	0.75	4.5	0.16

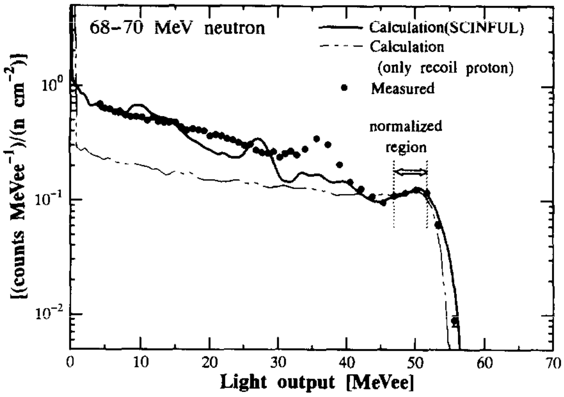

Fig. 23. Response function calculated using the SCINFUL code coupled with measured proton light yield data and normalized to measured response function for neutron energy 68–70 MeV. Dashed line is the result with our code which can calculate only recoil proton event.

yield. Fig. 23 exemplifies the result of SCINFUL calculation with revised light yield data and normalized to measured data for 68–70 MeV neutron.

The response matrix in the neutron energy of 0 to 120 MeV was formed by using the measured response functions from 5 to 120 MeV neutrons and the SCINFUL calculations below 5 MeV neutron. The lower limits of the measured light output data were 1.48, 2.63 and 4.59 MeVee for neutron energy range 5–33, 33–60 and 60–120 MeV, respectively. The values below these limits were obtained by smoothly connecting to the results calculated with the SCINFUL and CECIL codes.

Finally, we made the response matrix of 68 neutron bin $\times$ 70 light output bin from thus obtained response functions for neutron energy range up to 120 MeV. By using this matrix, we can obtain the neutron energy spectrum from the light output distributions with the unfolding method. We can distribute this response matrix on request.

7. Conclusion

The neutron response functions of 12.7 cm diam by 12.7 cm long BC501A were measured in the neutron energy range from 5 to 133 MeV with the TOF method in three cyclotron facilities, CYRIC, TIARA and RIKEN. By the help of calculation, the response function matrix was constructed for neutron energy up to 120 MeV. By using this matrix, we can unfold the pulse height distribution to neutron energy spectrum and obtain the accurate detector efficiency for energy range up to 120 MeV.

The calculated response functions were compared with the measured data, and the discrepancies were found above 30 MeV mainly owing to inaccurate light yields of charged particles. Especially, deuterons from C(n, d) reaction remarkably contribute to the response function, and the discrepancy between calculation and measurement become larger in the higher neutron energy. We could give the measured light yields of protons and deuterons for energy range up to around 120 MeV and the equation to present the light curves.

Acknowledgements

We wish to thank Dr. Atsuki Terakawa, Mr. Masashi Takada of CYRIC and Mr. Susumu Tanaka of TIARA, Dr. Takashi Ichihara, Mr. Shin Fujita, Mr. Shunji Nakajima of RIKEN, for their great help during the experiments in cyclotron facilities, and the cyclotron crews for their cyclotron operation. We would also like to express our appreciation to Prof. Tokushi Shibata of University of Tokyo and Prof. Kazuo Shin of Kyoto University for their helpful discussion and assistance in our study.

References

[1] R.E. Textor and V.V. Verbinski, ORNL-4160, Oak Ridge National Laboratory (1968).

[2] J.K. Dickens, ORNL-6463, Oak Ridge National Laboratory (1988).

[3] R.A. Cecil, B.D. Anderson and R. Madey, Nucl. Instr. and Meth. 161 (1979) 439.

[4] N.R. Stanton, COO-1545-92 (1971).

[5] Y. Uwamino, K. Shin, M. Fujii and T. Nakamura, Nucl. Instr. and Meth. 204 (1982) 179.

[6] V.V. Verbinski, W.R. Burrus, T.A. Love, W. Zobel, N.W. Hill and R. Textor, Nucl. Instr. and Meth. 65 (1968) 8.

[7] J.A. Lockwood, C. Chen, L.A. Friling, D. Swartz, R.N. St. Onge, A. Galonsky and R.R. Doering, Nucl. Instr. and Meth. 138 (1976) 353.

[8] K. Shin, Y. Ishii, Y. Uwamino, H. Sakai and S. Numata, Nucl. Instr. and Meth. A 308 (1991) 609.

[9] K. Shin, H. Tokumaru, M. Yoshida and T. Hyodo, Mem. Fac. Eng. Kyoto Univ. 41 (1979) 116.

[10] J.B. Birks, The theory and particle of scintillation counting (Pergamon, Oxford, 1964) p. 187.

[11] P.F. Rose and C.L. Dunford, ENDF/B-VI, National Nuclear Data Center, Brookhaven National Laboratory (1990).

[12] A.D. Guerra, Nucl. Instr. and Meth. 135 (1976) 337.

[13] V. McLane, C.L. Dunford and P.F. Rose, Neutron Cross Section, vol. 2, Neutron Cross Section Curves (Academic Press, 1988).

[14] T.W. Armstrong et al, ORNL-4869, Oak Ridge National Laboratory (1973).

[15] P. Kuijper, C.J. Tiesinga and C.C. Jonker, Nucl. Instr. and Meth. 42 (1966) 56.